

PAPER • OPEN ACCESS

Characterization of Damping Properties in 3D Printed Structures

To cite this article: Jenna Gietl *et al* 2018 *J. Phys.: Conf. Ser.* **1149** 012002

View the [article online](#) for updates and enhancements.



IOP | ebooks™

Bringing together innovative digital publishing with leading authors from the global scientific community.

Start exploring the collection—download the first chapter of every title for free.

Characterization of Damping Properties in 3D Printed Structures

Jenna Gietl¹, Joseph Vignola¹, Ph.D, John Sterling¹, Teresa Ryan², Ph.D

¹Center for Acoustics, Vibrations and Structures, Dept. of Mechanical Engineering, The Catholic University of America, Washington, DC

²East Carolina University, Department of Engineering
Greenville, NC 27858

E-mail: 02gietl@cua.edu

Abstract.

Current research on the effectiveness of a subordinate oscillator array (SOA) as a broadband mechanical filter relies on adequate knowledge of the SOAs material properties. Recent studies have shown a high sensitivity of these structures to disorder. A desire to produce large numbers of arrays to test this sensitivity to disorder motivated a transition from metal to 3-dimensional printed plastic SOAs. Irregularities associated with the curing process of the 3D printed polymers, as well as a general inconsistency of material properties of plastics, in turn highlighted the need for characterization of properties of 3D printed materials, especially those properties related to damping. As part of this study, several 3D printed plastic cantilevers, varying in material, printing technique, and printing orientation, are measured. Quantities of interest include the Young's modulus and density, as well as phenomenological properties, like the quality factor of specific designs. An ASTM standard test method for property determination is implemented with a laser Doppler vibrometer (LDV) to test each polymer. In addition to the ASTM protocol, tests are conducted in vacuum to distinguish internal damping mechanisms of the cantilever from external fluid mechanisms. Results are compared to both analytic and numeric predictions and published theory.

1. Introduction

Three-dimensional printing is increasing in popularity as new economical and efficient technologies are invented. Often engineers and architects utilize 3D printing because of its combination of high resolution and rapid prototyping. Beyond the scientific world, 3D printing has found its use in jewelry molds, custom manufacturing fixtures, and prop making [1]. As a relatively new technology, however, a thorough understanding of the properties of the materials produced by 3D printing is still emerging.

The authors have conducted a number of studies to understand and quantify different aspects of acoustic and vibrational damping [2, 3]. More recently, the apparent damping effect publicized by Soize [4] and later observed by Strasberg and Feit [5] is being investigated at CUA through the design of subordinate structures that, once attached to a primary structure, transfer energy [6, 7]. These subordinate structures are designed such that once the energy is transferred downscale away from the primary structure, it is dissipated in the subordinate array, essentially trapping the energy from the primary structure. The design of the subordinate array structure relies



on thorough knowledge of its material properties, specifically the Young's modulus and density, and a way to predict mode frequencies and damping for the system.

The literature on material properties, particularly those related to damping, of most 3D-printed polymers is largely inconsistent or lacking altogether. Therefore, further investigation of the effectiveness of 3D-printed mechanical filters requires quantification of the internal friction of the material. The purpose of this work is to use a standard testing protocol to determine material properties, especially those related to damping, of varying 3D-printed polymers. Specifically, modulus of elasticity, density, and properties related to damping will be addressed in this work. By measuring the resonance frequency and the density, the Young's modulus can be determined. The quality factor, Q , which is a measure of damping, can be calculated using the half-power bandwidth method.

In 3D printing, particularly stereolithography (SL), there are a number of fabrication variables both during and after material production that may contribute to inconsistencies in the final product. For example, printing technique, sample orientation during printing, printing temperature, post-printing curing time and wavelength, and post-printing wash time can all affect the material properties of a sample. Formlabs, a company that produces the stereolithograph apparatus (SLA) and the SLA used for this work, has investigated the effect of some of these variables, including post-curing UV wavelength [1] and geometric isotropy [8]. Each engineering resin produced by Formlabs was found to harden appropriately at a defined UV wavelength. Formlabs also claims that printing orientation does not affect material properties, particularly the Young's Modulus and tensile strength. In other words, unlike the anisotropy of the fused deposition modeling (FDM) technique, material properties are not direction-dependent.

2. Background

This study is motivated by previous and current research on damping by the authors. More recently, examination of the apparent damping effect [7] combined with piezoelectric control [9] has highlighted the need for characterization of damping of 3D printed materials.

Apparent damping is the dissipation of energy observed in a primary or master structure caused by subordinate attachments that draw energy away from the primary. This effect is seen in a tuned-mass-damper, in which a small mass is elastically attached to a larger primary mass and, if designed to have nominally the same resonant frequency as the primary, causes an effect similar to an electrical notch filter. Then, if several subordinate elements (rather than one) are attached to a primary, each designed to have an isolated natural frequency within a range of frequencies surrounding the resonant frequency of the primary, the apparent dissipation of energy from the primary is broadened across the range. The effect of attaching these subordinate elements for a specified mass ratio is analogous to applying an electrical band-rejection filter [6]. The subordinate oscillators are referred to here as a subordinate oscillator array, or SOA.

Counteracting the disorder sensitivity of these structures can be done by refining the design and production of each part. Design parameters that cause disorder are not discussed in this work, but production sensitivity is evaluated for various printing techniques. Using stereolithography, one of the many additive manufacturing/3D printing technologies available, small parts can be fabricated within a tolerance of one-hundredth of a millimeter, which is sufficient to counter disorder sensitivity. Stereolithography (SL) employs photopolymerization of liquid resins to build a solid polymer layer-by-layer. Once complete, ultraviolet curing fully hardens the structure [10]. This kind of additive manufacturing with curing produces a plastic with unique properties that vary with machine type, curing time and wavelength, and resin choice. Although material properties are provided for each resin, these fabrication variables result in large inconsistencies in the properties. Results from preliminary 3D printed SOA samples manufactured as print protocols were being developed showed up to 40% variation in

Young's modulus and quality factor from design to fabrication indicating the need for strict processing control and the possibility for sweeping variation when such processing (such as cure parameters) are not.

2.1. Samples

For this study, stereolithographic (SL) and fused deposition modeling (FDM) printing were the print methods used to produce samples. The primary difference between SL and FDM printing lies in the material state during printing. Stereolithography is a vat photopolymerization technique that uses UV light to partially cure material as each layer is laid down. Once the sample is fully printed, the material is in a green, or uncured, state and requires further UV curing to fully harden [10]. By contrast, FDM printing produces a part in its fully hardened state. Each of these methods differs with elements like strength of material, building volume, printing time, and material availability. One specific difference this work explores is isotropy of the printed material.

A secondary question addressed in this work is the effect of SL printing orientation on these properties. The material isotropy of stereolithography as discussed earlier is different than most 3D printing techniques. The FDM prints are anisotropic, or directionally dependent, because they are printed layer-by-layer without a post-print hardening process. With this technique, the bonds between layers are not as strong as those along a plane. However, because the layers of SL resins are not fully bonded before being cured, the bonds between layers harden at the same time as those along the plane. This technique produces an isotropic material. Therefore, the material properties are not expected to vary with respect to printing orientation. In the study of isotropy by Formlabs for their Form 2 printer, several specimens with an ASTM standard geometry were printed at orientation angles of 15 degree increments with respect to the xy-plane. Standard tensile tests indicated low error in Young's Modulus and yield strength between each sample [8]. The study by Formlabs concluded that strength of material is independent of printing orientation. The present work will compare results for vibrations samples and expand the study to determine whether damping is affected by build angle. The Young's modulus as well as resonance and damping properties will be compared for various printing orientations of SL samples.

2.2. Property Determination

One purpose of this work is to compare measured properties of seven 3D printed materials to the values provided by the manufacturer. Specifically, material properties, like the Young's Modulus and density, and phenomenological properties, such as the natural frequency and damping, of each sample will be determined experimentally. Each sample is designed through a finite-element, multiphysics simulation software, COMSOL, in which the dimensions and material properties are inputs. Combining our design with manufacturer-given material properties, this software predicts the eigenvalues, or bending modes, for each simple cantilever sample. These values are then used to assess the natural frequency of the part. As phenomena like the natural frequency and quality factor are dependent on these material properties, a comparison will be made between the given properties and predicted physical phenomena to measured values.

The density of each sample can be determined by the mass-volume ratio. Mass is measured on a scale, and the dimensions of the cantilever are measured with a digital caliper to calculate volume. The properties as designed are compared to those as printed in Table 1. These values indicate the accuracy of the printers by the percent difference, and the precision by the standard deviation.

The Young's modulus is often determined using well-known mechanical tests, such as the uniaxial tensile test or a three-point bending test. In such tests, Hooke's law is used to extract the modulus of elasticity in the elastic region on a stress-strain curve. For plastics, the elastic region

is very small; therefore, in this work, the Young's modulus will be determined by measuring the natural frequency. The relationship between natural frequency, density, and Young's modulus is shown in Eq. 1, where ω_n is the measured natural frequency of the cantilever, I_z is the mass moment of inertia, ρ is the density of the material, L and t are the length and thickness of the cantilever, $k_n L$ is the spatial frequency or wave number, and A is the cross-sectional area.

$$\omega_n = \frac{1}{L^2} \sqrt{\frac{EI_z}{\rho A}} (k_n L)^2 \quad (1)$$

Solving Equation 1 for the Young's modulus for a cantilever beam yields

$$E = \frac{1}{(k_n L)^2} \frac{12\rho L^4}{t^2} (\omega_n)^2 \quad (2)$$

Phenomenological properties, particularly damping, are the most difficult to predict because of the contributions of external factors. The quality factor is a measure of all damping of the material, both internal damping and external mechanisms, so damping itself is not a material property. However, by reducing damping to primarily internal mechanisms, a property-like attribute for a defined geometry and material can be determined. Damping can be quantified in various ways, so the quality factor will be used as the measure of damping for this thesis. A value representing damping can be extracted by measuring the frequency response of a beam and using the half-power bandwidth method for the first bending mode. Judge *et al.* define the quality factor of a damped material to be proportional to the ratio of the mechanical energy stored in the device to the energy shed per cycle of oscillation[2]. The shed energy in this case comes from a variety of internal and external mechanisms that draw energy from the resonator. External damping mechanisms include energy loss by attachment and a fluid environment. Attachment loss depends on the material, mass, and geometry of the affixed object and can be minimized by attaching a resonator with no common modes of energy. Fluid loss is present in different forms, depending on the fluid and geometry of the resonator. Fluid damping can be eliminated by placing the object in a vacuum.

Three dominant fluid mechanisms presented by Judge *et al.* include viscous damping, acoustic radiation loss, and squeeze film damping. Viscous loss, proportional to the square root of the fluid's pressure as seen in Eq. 3, dominates in denser fluids or in small enclosed environments. Acoustic loss, shown in Eq. 4 to be proportional to the fluid's pressure, also depends on fluid sound speed, resonator geometry, and the wavelengths of each. As its name suggests, squeeze film damping is significant for very narrow gaps between objects[11].

$$Q_{\text{viscous}} = \frac{t\rho_s}{3} \sqrt{\frac{\omega_n}{2\eta\rho}} \quad (3)$$

$$Q_{\text{acoustic}} = \frac{t\rho_s\omega_n}{2\sigma_r\rho c} \quad (4)$$

These external mechanisms in conjunction with internal damping form the total quality factor of the resonator. To isolate internal friction from external damping, each of these mechanisms is targeted in turn by different experimental approaches. Attachment loss is minimized by clamping each cantilever tightly to create a high impedance boundary. By placing the cantilever in a vacuum chamber with pressure on the order of milliTorr, fluid loss is reduced until it is insignificant.

3. Experimental Methods

3.1. Density

To determine the density of each material, the total mass of each sample is measured on an analytical balance. Using a digital caliper, the length, width, and thickness of both the cantilever beam and the head that holds the bolt hole are measured. The basic shape of the head and the cantilever is seen in Fig. 1. The volume of each sample is then extracted from these measured dimensions of the geometry; the sum of the volume of the cantilever and that of the head minus the bolt hole yield the total volume. Then, the ratio of mass to volume is compared to given values of density by the manufacturer.

3.2. Young's Modulus and Quality Factor

The Young's modulus and quality factor are determined from the same experiment, as both are extracted from measured phenomenological properties. The measured resonant frequency and its half-power bandwidth are used to calculate these two properties. By exciting each cantilever with energy in targeted frequency bands and measuring its response velocity with a laser Doppler vibrometer (LDV), damping of these 3D printed materials is characterized. Measuring 100 averages of the cantilever response reduces the signal to noise ratio and distinguishes the resonant frequency peak in the frequency domain. Then in MATLAB, a non-linear least-squares algorithm is used to fit the data to a Lorentzian function. This yields the center frequency, half-power bandwidth, and the quality factor, Q . An example of this curve fit is shown for an SL sample in Fig. 2.

3.3. ASTM Standard Requirements

ASTM Standard E756-05, the Standard Test Method for Measuring Vibration-Damping Properties of Materials, is implemented in this study [12]. Parameters regarding the shape, attachment, and excitation force of the samples are defined in this standard. The standard designates the use of a cantilever beam with a thickness to length ratio of, at minimum, 1:10. Two transducers are used in the experiment: one to provide a non-contact excitation force and one to measure (also without contact) the response. The non-contact force transducer in this experiment is an electrostatic force that is produced by sending a large DC offset voltage across

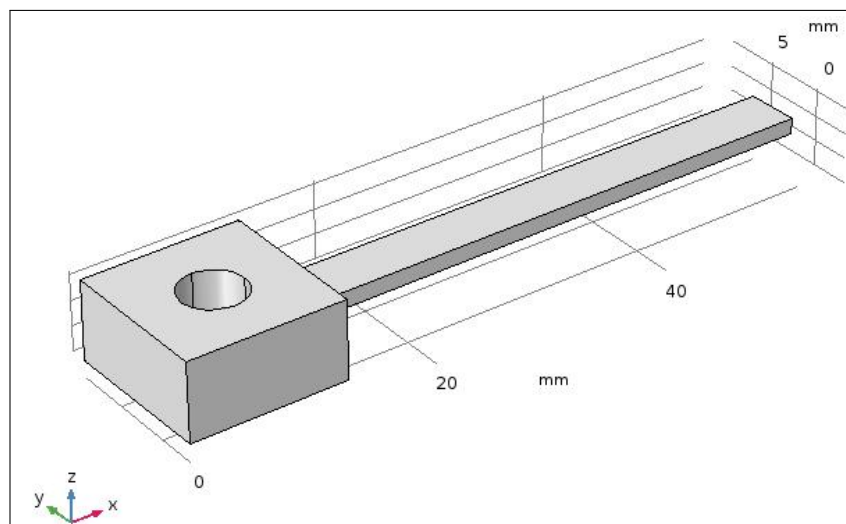


Figure 1: COMSOL is used to design the cantilevers with an attachment hole.

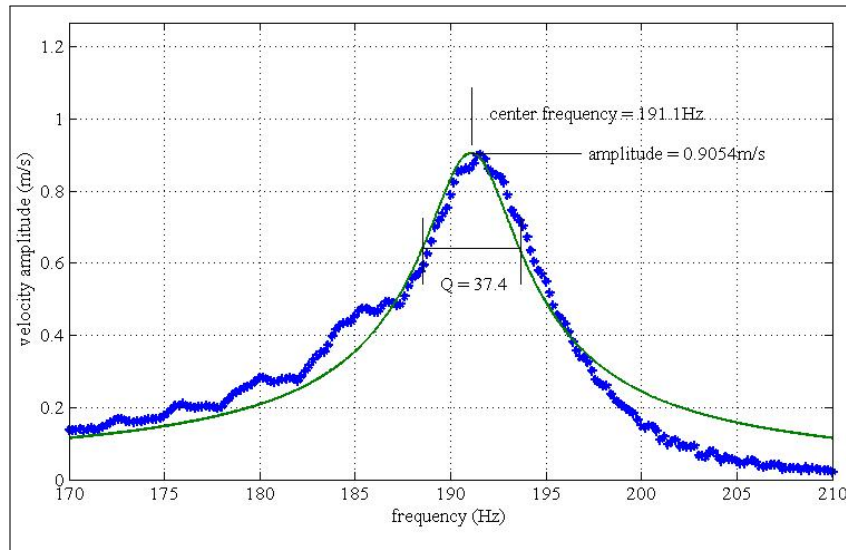


Figure 2: This figure shows the response of a gold-coated stereolithography cantilever to a 120-200 Hz chirp excitation.

a small gap between two conducting plates. One of the plates in this case is the cantilever, and the other is a thin plate of aluminum. For materials that are non-conductive or nonferrous, the standard suggests attaching “small bits of magnetic material...to the base beam side of the specimen to achieve specimen excitation and measurable response” [?]. To that end, sputter deposition was used to ionically bond a 35 nm layer of gold to the underside of the cantilever. As the aluminum sample is conductive, no gold was added.

3.4. Electrostatic force - F_s

An electrostatic force, F_s , is applied to the beam by grounding a plate that is positioned a very small distance below the beam. The cantilevers, which have been mutualized with a very thin layer of gold on the surface facing the grounded plate, are bolted to a high impedance mass. A voltage signal that has both an AC and DC component is then applied to the plate to produce the dynamic force in accordance with

$$F_S = \frac{A \cdot \epsilon_o}{2} \frac{(V_{ac} + V_{dc})^2}{r^2} \quad (5)$$

If only the static portion is considered, the remaining expression is

$$F_S = \text{area} \cdot \epsilon_o \frac{V_{ac} V_{dc}}{r^2} \quad (6)$$

where the permittivity of free space is $\epsilon_o = 8.854 \times 10^{-12} \frac{C^2}{Nm^2}$, r is the gap between the beam and electrode plate, and V is the total voltage [13].

3.5. Experimental Apparatus

As the focus in this experiment is to determine damping properties of each specimen, external fluid damping mechanisms will be reduced or eliminated by testing each sample within a vacuum chamber with pressure under 1 Torr. The sample, attached to a high impedance mass to reduce attachment loss, is bolted so that the majority of the cantilever hovers less than a millimeter

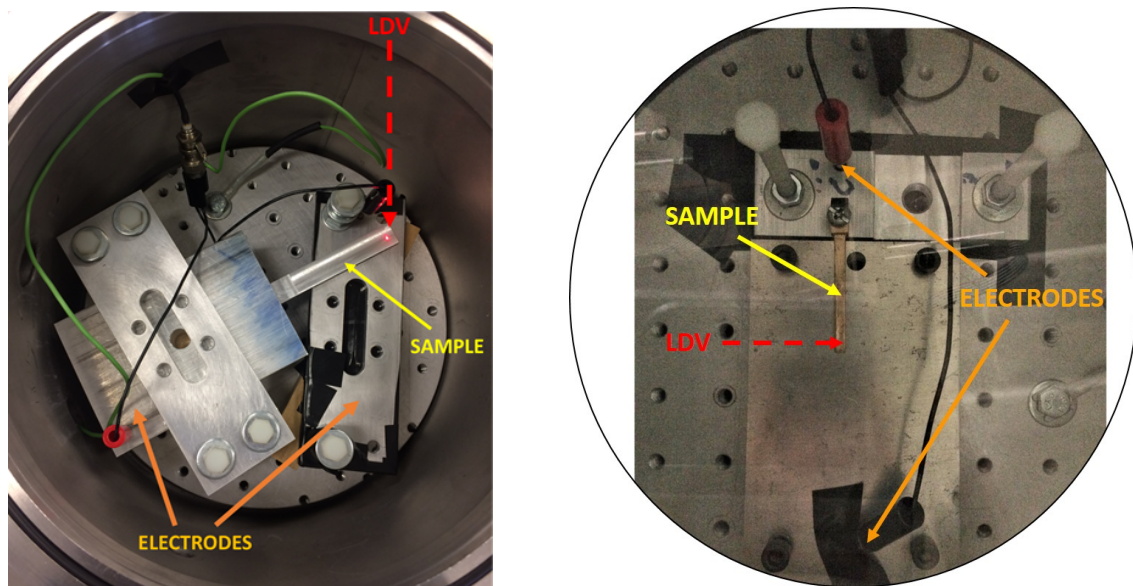


Figure 3: Bird's eye view of the vacuum chamber in which an aluminum (on the left) and then 3D printed (on the right) cantilever is attached to a high impedance mass and excited electrostatically.

above the conducting plate. Nylon non-conducting bolts secure the sample to the base plate of the vacuum chamber, and electrical tape separates the mass holding the cantilever from the base. The sample and high impedance mass act as a positive electrode, while the conducting plate and chamber are the ground component. Wires attached to each electrode connect the samples within the chamber to an external AC/DC amplifier. The electrostatic force that excites the sample is produced by a generated 1 V signal amplified with a gain of 14 dB and an offset of 200 V DC. The high impedance voltage between the sample and the conducting plate perturbs the sample enough that the laser Doppler vibrometer (LDV) can detect its vibration. The excitation signal used is a chirp for which the range of frequencies depends on the sample being tested. Using Eq. 2, the measured dimensions of each cantilever, and approximate values for density, an estimate of the natural frequency for each sample is calculated. The chirp is then designed with a 100-200 Hz range around the fundamental natural frequency to concentrate the energy in the first bending mode. Fig. 3 displays the two sample configurations; the first shows the aluminum cantilever machined from the large mass clamped to the vacuum base by a second plate. The second displays the 3D printed cantilever bolted to an aluminum block that is secured to the vacuum base. The cantilever hovers just above a plate whose four corner screws are attached to springs so that the plate can be adjusted to best fit the shape of the cantilever.

The beam from the laser Doppler vibrometer (LDV) shines directly onto the end of the cantilever through the glass lid of the vacuum chamber. Velocity data from the LDV measurement is collected by a National Instruments PCI-6221 with a sampling frequency of 10,000 samples per second and 100 averages of the signal. Time history and frequency spectra of the cantilever response are recorded. The schematic in Fig. 4 portrays the input and output of the signal and their connection to the physical components.

4. Results

The aluminum sample was tested first, as its material properties are well known. Using the same setup, the aluminum sample was tested with and without vacuum. The center frequency was estimated with material properties given by the manufacturer and measured dimensions

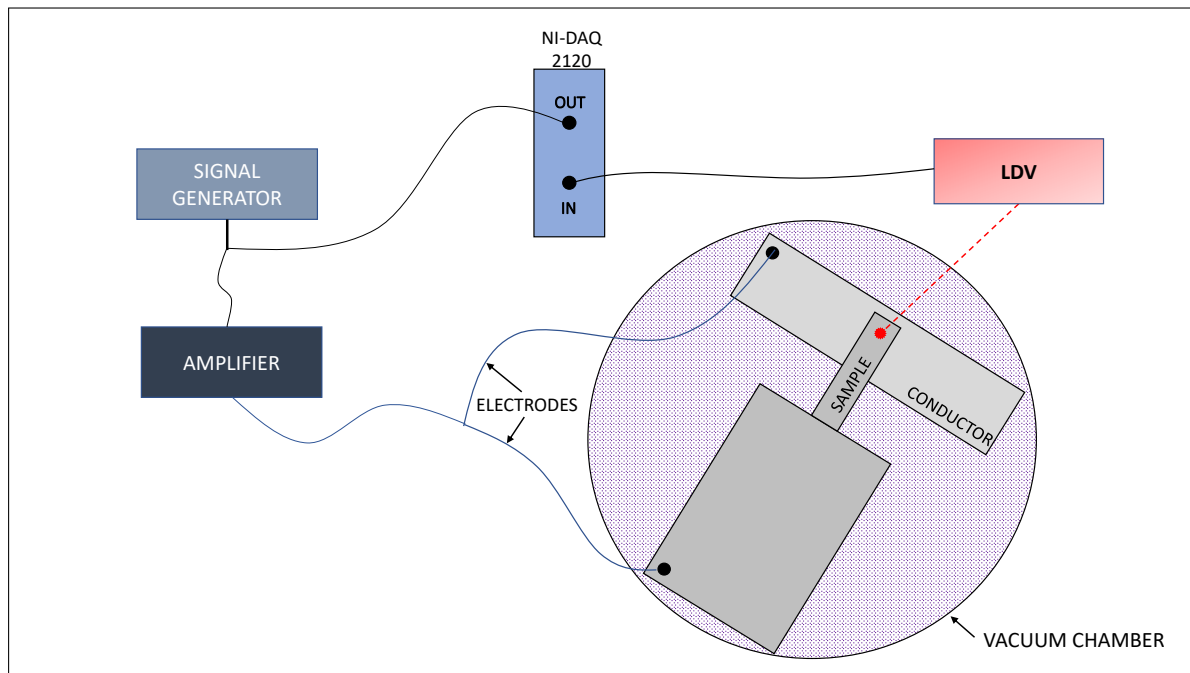


Figure 4: Top view of the experiment schematic indicating a generated input to excite the cantilever and a measured output from the LDV.

to have a value of 176 Hz. Therefore, a 120-200 Hz chirp was generated to concentrate the energy around the resonant peak. From the frequency response of the aluminum cantilever, the resulting center frequency of its resonant peak was found to be approximately 170 Hz. After curve fitting, the quality factor was found to be about 244 at ambient pressure (760 Torr), seen in Fig. 5, and 668 at a pressure of 900 milliTorr. The drastic increase in quality factor indicates that fluid damping plays a significant role for this oscillator.

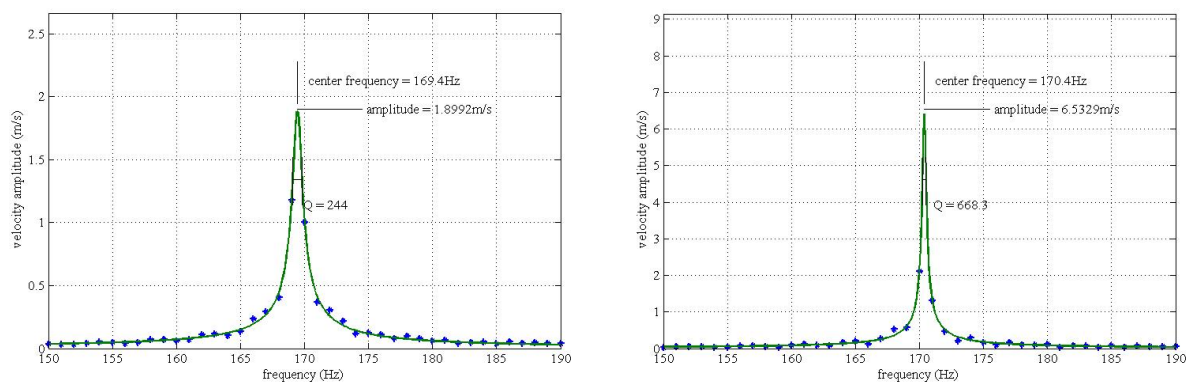


Figure 5: Each sample was tested and processed with identical excitation and curve-fitting limits in between trials with and without vacuum.

Sample	X Rotation (deg)	Y Rotation (deg)	Length (in)	Width (in)	Thickness (in)	Mass (g)
SL 1	0	45	1.672	0.163	0.0402	1.2805
SL 2	15	45	1.669	0.163	0.0488	1.3025
SL 3	30	45	1.660	0.163	0.0461	1.2908
SL 4	45	45	1.661	0.162	0.0476	1.3001
SL 5	60	45	1.665	0.163	0.0469	1.2877
SL 6	75	45	1.664	0.166	0.0469	1.3069
SL 7	45	15	1.663	0.162	0.0504	1.3019
SL 8	45	30	1.672	0.161	0.0472	1.2872
SL 9	45	60	1.670	0.163	0.0453	1.2751
Average	NA	NA	1.666	0.163	0.0466	1.293
DFA	NA	NA	0.28%	0.86%	%6.1	0.85%
As Designed	NA	NA	1.67	0.167	0.050	NA
% Difference	NA	NA	0.03%	2.28%	6.82%	NA

Table 1: Measured dimensions of the geometry and mass of the SL samples are displayed.

Sample	Density (kg/m^3)	Young's Modulus (GPa)	Center Frequency (Hz)	Q (no vacuum)	Q (vacuum)
SL 1	1086.9	2.22	180.4	20.7	23.8
SL 2	1043.3	1.39	179.1	20.6	23.0
SL 3	1051.4	1.56	176.0	20.9	22.0
SL 4	1036.2	1.44	178.3	19.5	23.8
SL 5	1043.2	1.55	179.6	19	25.1
SL 6	1063.2	1.58	180.6	21.2	24.7
SL 7	1034.3	1.16	171.1	18.1	21.1
SL 8	1074.8	1.44	171.1	20.3	22.3
SL 9	1057.2	1.67	175.8	19.7	22.5
Average	1054.5	1.56	176.9	20.0	23.1
DFA (%)	1.69	18.4	2.09	5.04	5.67
Calculated	1105	2.80	157	NA	NA
DFM (%)	4.57	270%	12.7%	NA	NA

Table 2: Material and phenomenological properties are determined for each printing orientation.

4.1. SL Samples

The measured dimensions and mass followed by calculated values of density, Young's modulus, center frequency, and quality factor are found in Tables 1 and 2. The results in Table 1 were used to determine the density and Young's Modulus of each sample given in Table 2. Fabrication error became increasingly evident as dimensions decreased—the thickness of the SL samples varied as much as 6.8% from the designed dimension. Compared to the manufacturer's values in Table 5, the average density of the tested samples had a percent error of 4.6% and the Young's modulus had an error of approximately 100%.

Table 2 displays the results of the properties found for each sample. Two kinds of error are observed here, which are defined as Deviation From Average (DFA) and Deviation From Manufacturer (DFM). The DFA is only considered for the SL samples as there are multiple

Sample	Length (in)	Width (in)	Thickness (in)	Mass (g)
Aluminum	3.0545	0.505	0.052	NA
ABS	4.145	0.410	0.132	17.179
CFN	4.163	0.407	0.143	18.153
FGN	4.157	0.405	0.135	16.403
PCF	4.153	0.405	0.131	19.255
PETG	4.194	0.413	0.139	21.907
PLA	4.180	0.409	0.139	19.294
Average	4.167	0.408	0.137	NA
DFA (%)	2.22%	0.81%	2.58%	NA
As Designed	4.167	0.417	0.125	NA
DFM (%)	0.003%	2.05%	9.24%	NA

Table 3: Measured dimensions and mass of the FDM samples are compared to those as designed.

samples printed from one material. For DFM, the mean of the property is compared to the property given by the manufacturer. This is the error observed for the FDM samples.

Overall, density for the SL cantilevers varied from the average (DFA) by 1.69%, Young's Modulus varied by 18.4%, resonant frequency varied by 2.09%, and quality factor varied by about 5%. Dividing the SL samples into two groups based on their printing orientation, those rotated in the X-direction and those rotated in the Y-direction, the same quantities are compared. For the six samples rotated about the x-axis, the density varied by 1.76%, Young's modulus varied by 19%, resonant frequency varied by 0.63%, and quality factor varied by 4.75%. Similarly, for the 4 samples rotated about the y-axis, density varied by 1.82%, Young's Modulus varied by 12.4%, resonant frequency varied by 0.63%, and quality factor varied by 4.91%. The modulus of elasticity is the most inconsistent of the properties but does not indicate orientation-based trends. It may be noted that the vacuum levels vary between 300 mTorr and 5 Torr. Constant peak vacuum was unattainable; however, as the quality factor of most of the samples only decrease by about 5-10% in most cases, it is reasonable to assume that fluid loss is not a dominant damping mechanism for these 3D printed plastics.

These results indicate that density, resonant frequency, and quality factor are sufficiently independent of printing orientation. The Young's modulus clearly varies per sample, but whether or not this can be attributed to printing orientation or sensitivity to fabrication error is unclear.

4.2. FDM Samples

The same tests imposed on the larger FDM samples produced more varied results. With only one sample per material, percent variation between samples cannot be estimated (DFA), but the percent error between the theoretical or estimated values and the measured values were compared (DFM). Table 3 displays the DFA and DFM for the FDM samples, both of which present error under 10% for the dimensions and mass. The error in these larger samples compared to that for the SL samples is significantly smaller. It is probable that the larger size of the samples allows for more accurate printing and therefore lower fabrication error.

The percent error between manufacturer and experimental values given in Table 4 indicate nearly 100% variation in Young's modulus and 10-50% error in density. Without a predicted value for any kind of damping per material, the quality factor is simply compared before and after vacuum. The percent difference in quality factor for four of the six samples is very low, at approximately 3-5%. However, for the ABS and PLA thermoplastics, Q varies more than 10% in vacuum, indicating a slightly higher sensitivity to fluid damping mechanisms.

Sample	Density (%)	Young's Modulus (%)	Q (%)
ABS	16.3	94	32.4
CFN	34.9	99	4.9
FGN	48.1	98	3.4
PCF	NA	100	4.0
PETG	11.8	95	4.7
PLA	22.5	95	11.1

Table 4: Density and Young's modulus DFM as compared to values provided in Table 5 are shown with the percent difference in quality factor with and without vacuum.

Sample	Density (kg/m^3)	Young's Modulus (GPa)
Aluminum	2700	69
ABS	1040	2.2
CFN	1400	54
FGN	1600	21
PCF	NA	54
PETG	1250	2.11
PLA	1270	3.5
SL Resin	1150	2.8

Table 5: Manufacturer-given values as available for density and Young's modulus. Found in material index on 3D Hubs webpage and in datasheets for each printer.

5. Conclusion

These results imply that the effect of printing orientation on stereolithographic prints is minimal. The Young's modulus for SL samples varied greatly from the manufacturer value. The large error in Young's modulus does not follow a trend with printing orientation, so more experiments must be done to determine the cause. Further investigations of these material properties, perhaps in which all fabrication variations are held constant, may help to explain the inconsistencies. Another study of interest would be to measure the frequency response as a function of vacuum level, particularly for the oscillators that had relatively large changes in damping when in vacuum.

The results of the fused deposition modeling samples indicated lower variation between designed and printed dimensions compared to the stereolithographic samples, which is likely due to the larger size of the FDM samples. The properties measured in this work of density and Young's modulus differed from manufacturer values significantly. The density was extracted directly from the measured dimensions and weight of each sample and diverged from literature up to 50% for some samples. The Young's modulus, which was calculated from the measured dimensions and the center frequency of each sample, had an even more extreme error of 90-100%. However, inconsistent data on material properties of 3D printed materials by different manufacturers makes this error less incriminating. The percent difference in quality factor with and without vacuum for the FDM samples is less than 5% for most of the materials, indicating low sensitivity to fluid damping.

For future work, continuing the study of 3D printed materials and their intrinsic properties by isolating specific aspects of the printing process will formulate a fuller characterization of these materials. Printing a large number of samples with constant design specifications would target fabrication disorder studies more directly. Once a baseline for fabrication disorder is

established (per printer, per material), investigations in unique 3D printing fabrication variables can be considered.

Acknowledgement

This work was supported in part by the NASA DC Space Grant Consortium Award 31377.

References

- [1] Formlabs. Form 2 tech specs.
- [2] John A. Judge, Douglas M. Photiadis, Joseph F. Vignola, Brian H. Houston, and Jacek Jarzynski. Attachment loss of micromechanical and nanomechanical resonators in the limits of thick and thin support structures. *Journal of Applied Physics*, 101(1):013521, January 2007.
- [3] John A. Judge, Joseph F. Vignola, and Jacek Jarzynski. Dissipation from microscale and nanoscale beam resonators into a surrounding fluid. *Applied Physics Letters*, 92(12):124102, March 2008.
- [4] C. Soize. Probabilistic structural modeling in linear dynamic analysis of complex mechanical systems, I - Theoretical elements. *La Recherche Aérospatiale (English edition)*, 5(-):Pages: 23–48, 1986.
- [5] Murray Strasberg and David Feit. Vibration damping of large structures induced by attached small resonant structures. *J. Acoust. Soc. Am.*, 99(1):335–344, 1996.
- [6] J.F. Vignola, J.A. Judge, and A.J. Kurdila. Shaping of a system's frequency response using an array of subordinate oscillators. *Journal of the Acoustical Society of America*, 126:129–139, 2009.
- [7] Joseph Vignola, Aldo Glean, John Judge, and Teresa Ryan. Optimal apparent damping as a function of the bandwidth of an array of vibration absorbers. *The Journal of the Acoustical Society of America*, 134(2):1067–1070, August 2013.
- [8] Formlabs. Validating Isotropy in SLA 3d Printing, October 2016.
- [9] Sai Tej Paruchuri, John Sterling, Andrew Kurdila, and Joseph Vignola. Piezoelectric composite subordinate oscillator arrays and frequency response shaping for passive vibration attenuation. In *Control Technology and Applications (CCTA), 2017 IEEE Conference on*, pages 702–707. IEEE, 2017.
- [10] Formlabs. Ultimate Guide to Stereolithography.
- [11] Joseph F. Vignola and John A. Judge. Architectural considerations of micro- and nanoresonators for mass detection in the presence of a fluid. *Journal of Applied Physics*, 104(12):124305, December 2008.
- [12] ASTM E756-05, Standard Test Method for Measuring Vibration-Damping Properties of Materials, 2017.
- [13] Subrahmanyam Gorthi. *Characterization of MEMS Electrostatic Actuators Beyond Pull-In*. PhD thesis, Indian Institute of Science, Bangalore, January 2006.